Materialia 15 (2021) 100979

Contents lists available at ScienceDirect

Materialia

journal homepage: www.elsevier.com/locate/mtla

Full Length Article

Oxygen vacancies in zirconium oxide as the blue luminescence centres and traps responsible for charge transport: Part I—Crystals

Damir R. Islamov[a,b,*], Vladimir A. Gritsenko[a,b], Timofey V. Perevalov[a,b], Alexander P. Yelisseyev[c], Vladimir A. Pustovarov[d], Ilya V. Korolkov[e,b], Elena E. Lomonova[f]

[a] Rzhanov Institute of Semiconductor Physics SB RAS, 13 Lavrentiev Avenue, Novosibirsk 630090, Russian Federation
[b] Novosibirsk State University, 2 Pirogov Street, Novosibirsk 630090, Russian Federation
[c] Sobolev Institute of Geology and Mineralogy SB RAS, 3 Koptyug Avenue, Novosibirsk 630090, Russian Federation
[d] Experimental Physics Department, Ural Federal University, 19 Mira Street, Yekaterinburg 620002, Russian Federation
[e] Nikolaev Institute of Inorganic Chemistry SB RAS, 3 Lavrentiev Avenue, Novosibirsk 630090, Russian Federation
[f] Prokhorov Institute of General Physics RAS, 38 Vavilov Street, Moscow 119991, Russian Federation

ARTICLE INFO

Keywords:
Zirconium oxide
Defects
Oxygen vacancy
Luminescence
DFT

ABSTRACT

The origin of luminescence centres in ZrO_2 crystals was studied using Raman scattering, luminescence spectroscopy and quantum-chemical calculations. The 2.7 eV luminescence band and 5.2 eV absorption/luminescence excitation band are associated with an oxygen vacancy. It was shown, that a half of the Stokes shift in blue photoluminescence spectra is equal to the trap thermal activation energy 1.25 eV. Within quantum-chemical simulations it was demonstrated that both electrons and holes can be trapped on oxygen vacancies in ZrO_2. Hence, oxygen vacancies are supposed to operate as traps responsible for the blue luminescence band in ZrO_2.

1. Introduction

Crystalline and amorphous materials based on pure and doped zirconium dioxide are of significant interest from a scientific viewpoint, as well as from a practical point of view. The relevance of creating such materials is determined by the prospects for their use as oxygen-exchange membranes in fuel cells, sensors and other similar devices, as well as structural non-metallic wear-resistant materials [3–7]. Due to a high melting temperature (≈ 2900°), such materials can be used for the manufacture of structural parts operating under extreme conditions of high mechanical loads, chemically aggressive environments, elevated temperatures, in the absence of lubrication, etc. Zirconia-based materials are used for the manufacture of tools with a great cutting edge sharpness, both for high-precision processing of various materials (metal, wood, glass, crystals, etc.), and for high-quality medical instruments with cutting edge thickness values up to 100 nm for cardio and neurosurgery, vascular, maxillofacial surgery and ophthalmology [28]. The bio-inertness of this material makes it promising when used in medicine for tooth implants [16,27].

The noticeable optical and mechanical properties of zirconia crystals and ceramics combined with the unique ability to modify the characteristics of the material by introducing a number of activating impurities, open up great opportunities for using stabilized zirconia as active and passive laser elements [8,35].

At present, there is a generally accepted hypothesis that oxygen vacancies play a crucial role in the mechanical and optical properties of ZrO_2 crystals. There are a lot of theoretical investigations of oxygen vacancies electronic structure in ZrO_2 [1,2,9,17,32]. A blue band with an energy of about 2.7 eV is observed in the luminescence spectra of ZrO_2 [2,21,22,37]. Despite the fact that main hypothesis is that the oxygen vacancies in ZrO_2 crystals is related with this luminescence band, the nature of this luminescence band is a matter of debate. For example, it was shown that the 2.7-eV-blue luminescence band in HfO_2 (Hf and Zr have an isoelectronic structure of valence shells) is related to oxygen vacancies [12]. However, recently, it has been concluded that the blue luminescence band is not related to oxygen vacancy in ZrO_2 crystals and films [21,22].

The aim of the present research is to identify the origin of the blue (2.7–2.8 eV) luminescence band in ZrO_2 crystals.

2. Experimental methods

2.1. Preparation of samples

Zirconium oxide crystals were obtained using a directed melt crystallization at a high-frequency dielectric heating within the 'Kristall-407' installation (the frequency is 5.28 MHz, maximum output power is

* Corresponding author at: Rzhanov Institute of Semiconductor Physics SB RAS, 13 Lavrentiev Avenue, Novosibirsk 630090, Russian Federation.
E-mail address: damir@isp.nsc.ru (D.R. Islamov).

https://doi.org/10.1016/j.mtla.2020.100979
Received 13 April 2020; Accepted 30 November 2020
Available online 4 December 2020

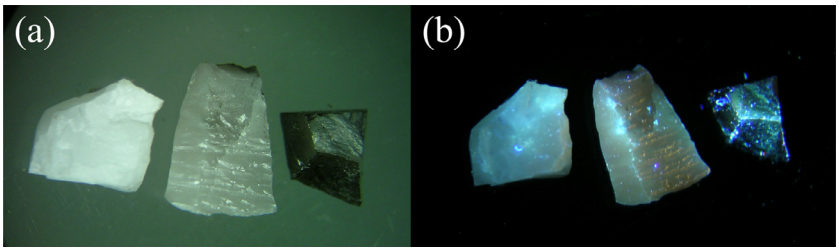

Fig. 1. ZrO_2 crystal samples: (a) appearance, (b) photoluminescence pattern. Three samples are shown from left to right: without annealing treatment, after the annealing in vacuum at 1600° and 2100°.

60 kW) with the 130 mm diameter of the water-cooled copper melting pot [26]. The batch loading mass was 6 kg. Zirconium oxide powders with the basic substance content of at least 99.99% were used to prepare the batch. Directed melt crystallization was carried out by lowering the melting pot with the melt relative to the inductor at the speed of 10 mm/h. The as-grown crystals are white and opaque, have a needle shape and cross-sectional dimensions of 3–7μm.

The examples of (poly-)crystal pieces are shown in Fig. 1(a): without annealing and after the annealing in vacuum at 1600° and 2100°. The heat treatment of crystals after their growth was carried out in 10^{-4} Torr vacuum at the temperatures of 1600° and 2100° for 2 h. After the annealing at 1600°, the crystals darkened somewhat, whereas after the heat treatment at 2100°, the samples turned black. Recently, the darkening of ZrO_2 crystals and visible-range growing of the optical absorption band were described by the oxygen depletion after high-temperature annealing on the ZrO_2 crystals [26]. Also, the directed melt crystallization leads to the significant decreasing of impurities content (e.g. from the initial level of 5×10^{-3} to 10^{-4}–10^{-5} vol% after the heat treating) [26]. As far as the 'Kristall-407' installation is equipped with a molybdenum furnace without carbon parts, the darkness in not related with the carbon implantation into ZrO_2 crystals. Moreover, a carbon holder enhances ZrO_2 recovery without introducing carbon due to the increased volatility of carbon oxides at high temperatures [26].

2.2. XRD measurements and analysis

XRD analysis of polycrystals was performed on Shimadzu XRD-7000 diffractometer (CuK-α radiation, Ni-filter, linear One Sight detector, 5–70°2θ range, 0.0143°2θ step, 2 s per step). A polycrystalline sample was slightly ground with hexane in an agate mortar, and the resulting suspension was deposited on the polished side of a standard quartz sample holder, a smooth thin layer being formed after drying. Indexing of the diffraction patterns was carried out using data for compounds reported in the PDF database [Powder Diffraction File, release 2010, International Centre for Diffraction Data, Pennsylvania, USA].

2.3. Optical measurements

Raman spectra were collected at room temperature on a LabRAM HR microRaman spectrometer using a 532 nm Nd:YAG solid state laser, with a spot size ~5 μm. The integration and accumulation times were 3 s. The measurements were replicated at five points to check their reproducibility.

A DDS400 deuterium lamp and primary double-prism monochromator DMR-4 were used for the photoluminescence (PL) excitation (PLE). The PL spectra were recorded using a secondary DMR-4 double-prism monochromator and a Hamamatsu R6358-10 type photomultiplier tube. The PLE spectra were normalized to the equal number of photons incident on the sample using a yellow lumogen, which is a luminophore with the known energy quantum yield over the studied spectral range. The PL emission spectra were not corrected for the spectral sensitivity of the registration system.

The X-ray excited luminescence (XRL) spectra were measured at room temperature using an MDR2 diffraction monochromator (LOMO, St. Petersburg) and an FEU-100 photomultiplier as an emission detector.

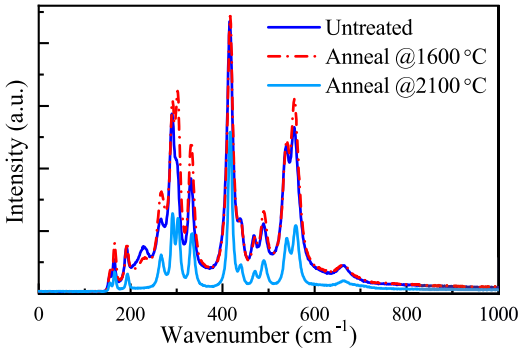

Fig. 2. The Raman spectra for ZrO_2 crystals before and after annealing.

The luminescence was excited using a tabletop X-ray URS1.0 machine containing a BSV-2W tube with the W-anode (40 kW, 20 mA).

Thermally stimulated luminescence (TSL) curves were obtained using a liquid nitrogen vacuum cryostat, where the sample was located on a cold conductor. The samples were excited at the liquid nitrogen temperature by the UV irradiation at $\lambda = 365$ nm from a DRSh100.2 mercury lamp. The TSL curves were recorded during the samples heating in the dark at the rate of $\beta = 20$ K/min. The TSL radiation was recorded in the spectral range of 400–800 nm within a photomultiplier tube FEU-100. Radiation 365 nm (3.4 eV), picked out using a UFS6 filter from the Hg lamp spectrum, excites photoluminescence (PL) in the range 400–800 nm (1.5–3.1 eV). Additionally, in order to ionize the oxygen vacancy in ZrO_2, the samples were irradiated with X-rays.

2.4. Ab-initio simulations

The ZrO_2 electronic structure was investigated within the density functional theory with the BPE0 exchange-correlation functional. The plane-wave cutoff energy was taken equal to 70 Ry, and the potentials of nuclei and core electrons were described by optimized norm-conserving Vanderbilt pseudopotentials [14,15]. The oxygen vacancies were simulated by removing an oxygen atom from the 96-atom supercell of monoclinic (m-) ZrO_2, respectively. The simulations were carried out using the Quantum ESPRESSO code [11]. The crystal structure and charge density spatial distribution visualizations were made within the XCrySDen software [25].

3. Results

3.1. Crystal structure identification

3.1.1. Raman spectra

The Raman spectra for ZrO_2 before and after annealing are shown in Fig. 2. ZrO_2 exhibits different crystal modifications, among which, under normal conditions, monoclinic phase m-ZrO_2 is stable. At the temperature of 1170°, m-ZrO_2 is transformed into the tetragonal t-ZrO_2 phase, which, in turn, becomes c-ZrO_2 at $T > 2370$°. Phase transformation of m-ZrO_2 was observed under heavy ion irradiation [36]. The Raman spectra in Fig. 2 are characteristic for m-ZrO_2 [33]. During the annealing with a

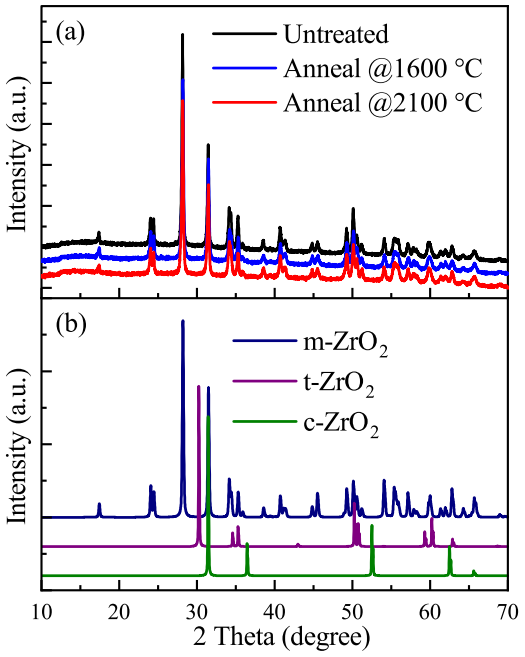

Fig. 3. XRD spectra of the ZrO_2 crystals. (a) Experiment data for ZrO_2 crystals before and after annealing. (b) Calculated data from ICSD using POWD-12++: m-ZrO_2 PDF 010-83-0939 (Bondars, B., Heidemane, G., Grabis, J. and Lasch, 1995), t-ZrO_2 PDF 010-70-6627 (Bouvier, P., Djurado, E., Lucazeau, G. and Le-Bi, 2000) and c-ZrO_2 PDF-010-70-6632 (Bouvier, P., Djurado, E., Lucazeau, G. and Le-Bi, 2000).

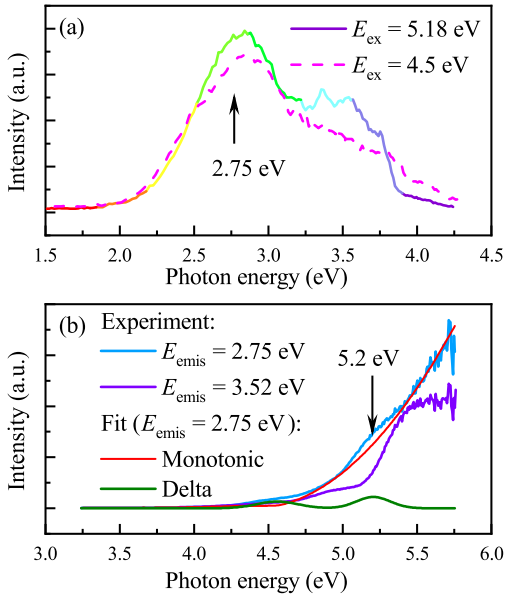

Fig. 4. (a) The ZrO_2 PL spectra with the excitation energies of 5.18 eV and 4.5 eV. The arrow shows the position on the main peak in the PL spectra. (b) The ZrO_2 PLE spectra for emission energies 2.75 (blue) and 3.52 eV (violet). The red line represents the monotonic component of the blue curve; the difference between the blue and red curves is shown in olive.

following cooling to room temperature, possible phase transitions to t-ZrO_2 or c-ZrO_2 are not observed. These results are in agreement with the fact that undoped ZrO_2 single crystals cannot keep phases with higher symmetry than monoclinic one if they were cooled naturally to room temperature.

3.1.2. XRD analysis of crystals

To clarify the question with the phase transformation, additional experiments were carried out on XRD analysis of the ZrO_2 crystals. The XRD spectra of the initial (black line) ZrO_2 and after annealing (blue and red lines) in Fig. 3(a). The data from the PDF bank for different ZrO_2 phases are shown in Fig. 3(b). One can see that, all samples are single phase monoclinic ZrO_2.

3.2. Defect nature identification: optical methods

3.2.1. Photoluminescence

In addition to the general appearance of ZrO_2 crystals in Fig. 1(a), the photoluminescence patterns for them before and after the annealing at high temperatures are shown in Fig. 1(b). One can see that all samples exhibit blue luminescence. The PL spectrum of untreated ZrO_2 excited by a 5.18 eV quantum is shown in Fig. 4(a). The peak with an energy of 2.75 ± 0.05 eV (blue luminescence peak) dominates in the PL spectrum. A less intense luminescence is observed in the ultraviolet (UV) region of the spectrum near the photon energies of 3.5 eV.

In Fig. 4(b) is the ZrO_2 excitation spectrum of blue photoluminescence with the energy of 2.75 eV. In the PLE spectrum of the blue PL band, two shoulders are observed at the energies of about 5.2 eV and 4.5 eV. The monotonic component of the PLE spectra is shown by a red line. It was obtained as a part of the following function:

$$I \sim (h\nu - \tilde{E})^x + g_1(h\nu) + g_2(h\nu),$$

where I is total PLE intensity, $h\nu$ is photon energy, $\tilde{E}$ is a variable parameter, x is a power constant, $g_{1,2}(h\nu)$ are the Gauss functions. The fitting procedure returned the power value $x \approx 2$ and $\tilde{E} \approx 4.4$ eV. The difference between the full PLE spectra and monotonic component is shown by an olive curve that is fitted by the first Gaussian with the centre at 4.559 ± 0.001 eV and variance 0.28 ± 0.006 eV, and the second Gaussian with the centre at 5.22 ± 0.003 eV and variance 0.3 ± 0.07 eV. One can see that the 2.7–2.8 eV PL band is excited by photons with energies of 4.56 eV and 5.2 eV. The PL spectrum of untreated ZrO_2 excited by a 4.5 eV quantum is shown in Fig. 4(a) by a magenta line, which exhibits a main peak near 2.75 eV as well as 5.18-eV-excited PL. Recently, it has been concluded that the 4.2-eV-excited blue luminescence band is not related to oxygen vacancy in ZrO_2 and caused by the inter-band absorption [22].

The UV PL (3.52 eV) is excited by 5.5 eV photons, as shown by a violet curve in Fig. 4(b). One can see that the 5.5 eV PLE maximum is absent in the 2.75 eV emission excitation spectrum. Thus, the 3.5 eV PL has the nature different from the 2.7–2.8 eV band.

Annealing do not change the shape of PL spectra, but intensity of the 2.75 eV peaks increases (not shown).

The PL and PLE spectra of slightly non-stoichiometric zirconium oxide films depleted in oxygen (enriched in zirconium) were shown in Ref. [27]. The oxygen vacancy in ZrO_2 exhibits an absorption peak at an energy of about 5.2 eV.

The maximum absorption energy of the oxygen vacancies in zirconium oxide coincides with the maximum excitation energy of the blue luminescence band, as shown in Fig. 4(b) and in Ref. 27. Thus, one can conclude that the oxygen vacancies in ZrO_2 are defects that responsible for the 2.7–2.8 eV blue PL band, which is excited by photons with an energy of about 5.2 eV.

The configuration diagram of optical transitions at a neutral oxygen vacancy in ZrO_2 is shown in Fig. 5. The lower term corresponds to the ground occupied state, the upper term corresponds to an empty excited state. The vertical transition with the energy of 5.2 eV corresponds to the transition from the ground to the excited state. The reverse transition with the energy of 2.7 eV corresponds to the radiative transition (blue luminescence). It should be noted that half of Stokes blue luminescence shift $(5.2 - 2.7)/2 = 1.25$ eV is equal to the thermal trap energy determined from the charge transport in ZrO_2 films as described in Ref. [19].

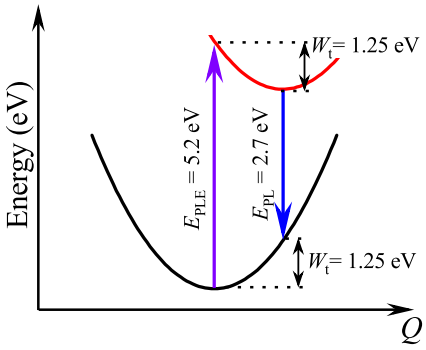

Fig. 5. Configuration coordination energy diagram of optical transitions at a neutral oxygen vacancy in ZrO_2. The arrows indicate the optical transition with the energy of 5.2 eV from the ground filled state (black curve) to the excited empty state (red curve),and the radiative PL transition with the energy of 2.7 eV.

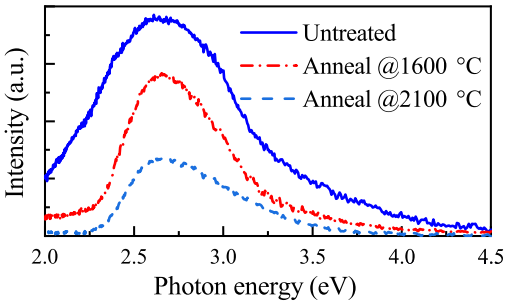

Fig. 6. The ZrO_2 XRL spectra before and after annealing.

3.2.2. X-ray excited luminescence

In Fig. 6 are the X-ray excited luminescence spectra of the untreated ZrO_2 crystals and ones after the annealing at 1600° and 2100°. The XRL spectra are dominated by a luminescence maximum with an energy of about 2.7 eV. The additional bands of both low and high energy sides are also observed. High-energy ones are present for all three samples, while low-energy components are characteristic only for an unannealed ZrO_2 crystal.

One can see that the maximum intensity is intrinsic to the white initial samples. High-temperature annealing leads to the darkening of crystals, and the XRL intensity decreases with the increasing annealing temperature. It should also be noted that the darkening of crystals during X-ray irradiation takes place. These phenomena might take place due to the effect of concentration quenching, when an increase of defect density leads to a decrease in the luminescence intensity [18,23].

As far as the XRL maximum intensity is located near 2.7 eV, it can be concluded that oxygen vacancies are responsible for XRL, as well as for the blue PL band.

3.2.3. Thermally stimulated luminescence

The TSL curves for untreated ZrO_2, as well as ZrO_2 samples after the annealing at 1600° and 2100°, are shown in Fig. 7(a). On the TSL curves, one can observe the dominant peak at about 260 K and 7 weak peaks in the temperature range of 100–550 K, which maximum positions T_m are shown in Table 1.

High-temperature annealing of crystals is accompanied by the quenching of thermoluminescence, similar to that takes place in the X-ray luminescence spectra. Major peaks remain. They are relatively symmetrical, and it corresponds to the 2nd order of kinetics. The TSL curve for untreated ZrO_2 was decomposed with the TSL signal maxima. We

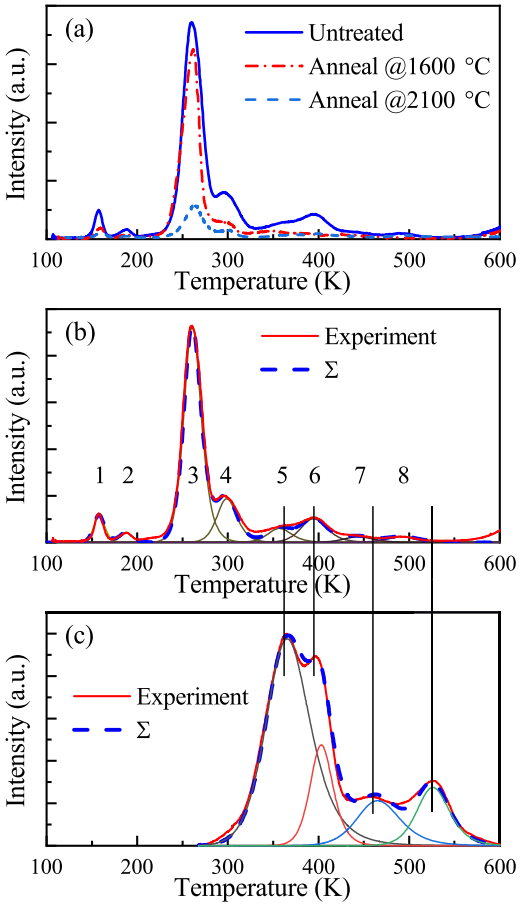

Fig. 7. The ZrO_2 TSL spectra after the 365-Hg excitation. (a) The TSL for crystals before and after annealing. (b) The experimental TSL curve recorded for the untreated ZrO_2 crystal (red solid line) and results of the TSL curve decomposition into individual peaks following the Eq. (1) (thin lines); the dashed line shows the sum of 1–8 individual peaks. (c) The experimental TSL curve recorded for the untreated ZrO_2 crystal (red solid line) after X-ray excitation at room temperature and results of the TSL curve decomposition into individual peaks following the Eq. (1) (thin lines); the dashed line shows the sum of individual peaks. Vertical thin black lines are eye-guides.

Table 1
The positions of the TSL peaks T_m and the calculated thermal activation energies W_t with frequency factors ν under the assumption of the second order kinetics.

#	T_m (K)	W_t (eV)	ν (s^{-1})
1	158	0.52	3.54×10^{15}
2	187	0.62	3.54×10^{15}
3	261	0.87	3.53×10^{15}
4	299	1.00	3.52×10^{15}
5	357	1.20	3.51×10^{15}
6	395	1.33	3.51×10^{15}
7	444	1.50	3.52×10^{15}
8	493	1.67	3.46×10^{15}

followed the Garlick–Gibson formula [10]

$$I(T) = \frac{n_0 \nu \exp\left(-\frac{W_t}{kT}\right)}{\left(1 + \frac{\nu}{\beta}\int_{T_0}^{T} \exp\left(-\frac{W_t}{kt}\right)dT\right)^2}$$

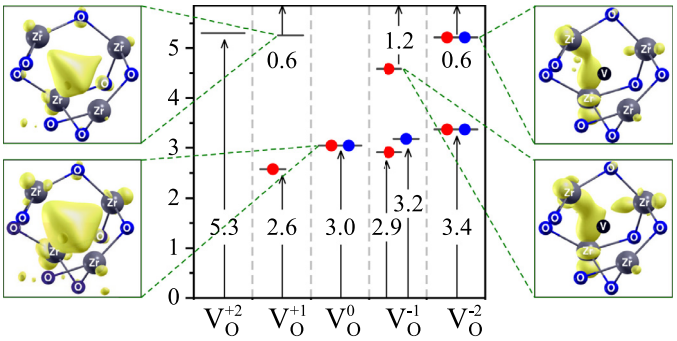

Fig. 8. Defect energy levels in the bandgap for five charge states of the 4-coordinated oxygen vacancy in m-ZrO_2. In the insets are the spatial charge density distributions for appropriate defect levels. Numeric values are specified in eV.

that can be simplified to the following expression [24]:

$$I(T) = \frac{I_m \exp\left(\frac{W_t}{kT}\frac{T-T_m}{T_m}\right)}{\left[\frac{T^2}{T_m^2}(1-\delta)\exp\left(\frac{W_t}{kT}\frac{T-T_m}{T_m}\right)+1+\delta_m\right]^2}, \quad (1)$$

where n_0 is the initial density of trapped electrons, T_0 is the initial temperature, I_m is the TSL peak amplitude, $\delta = 2kT/W_t$ and $\delta_m = 2kT_m/W_t$. The parameter values of W_t and ν, calculated for 8 components following Eq. (1), are given in Table 1. There is a good agreement between the sum of these components and the experimental curve in Fig. 7(b).

It should be noted that, at temperatures of 361 and 395 K, there are the TSL peaks, corresponding to the trap energies of 1.2 and 1.33 eV, which are close to 1.25 eV, as well as the frequency factors $\nu = 3.5 \times 10^{15}$ s^{-1} which are determined from the charge transport in ZrO_2 films using Eq. (10) and results in Ref. [19]. The experimental TSL curve recorded for the untreated ZrO_2 crystal after X-ray excitation at room temperature are shown in Fig. 7(c). One can see that the first two main peaks in Fig. 7(c) corresponds to peaks 5 and 6 of Hg-excited TSL in Fig. 7(b). It means that the set of trapping centres does not depend on the excitation wavelength (X-ray or 365-Hg lamp). In conclusion, the TSL peaks at 361 and 395 K are highly likely correspond to the oxygen vacancies, while the nature of other peak requires to be investigated additionally.

3.3. *Defect nature identification:* ab initio *simulations*

The single-electron Kohn–Shem level positions in the m-ZrO_2 bandgap produced by the 4-coordinated (as having a smaller formation energy) oxygen vacancy (V_O) in different charge states are shown in Fig. 8. The neutral V_O gives a level in the middle of the bandgap, filled by two electrons which are localized at the oxygen vacancy site. This is a well-known result [9,17]. In the positively charged V_O^{+1}, there is a single-occupied level above the valence band top E_v at 2.6 eV, and an empty level below the conduction band bottom E_c at 0.6 eV. The spatial charge density distribution in that case is localized around the vacancy site evenly between the nearest Zr atoms, like at the neutral V_O level as shown in the insets to Fig. 8. The strong charge localization at the vacancy site centre due to the polaronic effect has a typical structure of an *F* centre. An electron addition to the structure results in the appearance of a second single filled level in the bandgap at 1.2 eV below E_c. The spatial charge from the added electron is distributed primarily between two Zr atoms that are nearest to the V_O centre, demonstrating the binding nature of the charge density distribution. Two electrons added to the supercell form two filled levels. The upper one is 0.6 eV below E_c. The charge density distribution for this level is similar, but a little weaker than for the upper level from a negatively charged The energy value accuracy in Fig. 8 is about 0.1 eV due to the use of different exchange-correlation functionals and pseudopotentials. Thus, the obtained picture of the Kohn–Shem level positions from V_O in the m-ZrO_2 bandgap are close to that obtained earlier [17,31].

4. Discussion

HfO_2 and $Hf_{0.5}Zr_{0.5}O_2$ exhibit the blue luminescence band with the energy of 2.7 eV [12,13,20,23,29,34]. The blue luminescence band in HfO_2 and $Hf_{0.5}Zr_{0.5}O_2$ has the excitation peak at the energy of 5.2 eV [20,29]. Similar optical properties we observed in ZrO_2 crystals in the present work. The quantum chemical simulations show that the oxygen vacancies in ZrO_2, as well as in HfO_2 and $Hf_{0.5}Zr_{0.5}O_2$ as described in the literature, have the absorption band at the energy 5.2 eV. Hence, the oxygen vacancies in ZrO_2 (HfO_2, $Hf_{0.5}Zr_{0.5}O_2$) are responsible for the blue luminescence band. The thermal trap energy in ZrO_2, HfO_2 and $Hf_{0.5}Zr_{0.5}O_2$ is equal to 1.25 eV, and it is equal to half of the Stokes blue luminescence shift (5.2 – 2.7)/2 = 1.25 eV in ZrO_2 crystals. Hence, one can conclude that the oxygen vacancy is the defect responsible for the blue luminescence in ZrO_2 crystals as well as in ZrO_2, HfO_2 and $Hf_{0.5}Zr_{0.5}O_2$ films [12,20,30].

5. Conclusion

In conclusion, the defect nature in ZrO_2 crystals was studied with Raman spectroscopy and photoluminescence spectroscopy, thermally stimulated spectroscopy and quantum chemical simulations. It was established that the blue luminescence band with an energy of about 2.7–2.8 eV and the excitation bands with the energy of 5.2 eV are due to the oxygen vacancy in ZrO_2. According to the literature data, the blue luminescence band excited by 4.2–4.5 eV photons is caused by the interband absorption. The thermal $W_t = 1.25$ eV trap energy in ZrO_2 was determined, which is equal to half of the Stokes shift of blue luminescence. It was be concluded that the oxygen vacancies in ZrO_2 are responsible for the blue luminescence. The nature of other PL and TSL bands are unknown, this question still waits to be resolved.

Author information

ORCID
Damir R. Islamov: 0000-0002-5188-7049
Vladimir A. Gritsenko: 0000-0003-1646-0848
Timofey V. Perevalov: 0000-0003-0895-6202
Alexander P. Yelisseyev: 0000-0002-0509-2122
Vladimir A. Pustovarov: 0000-0001-7373-1152
Ilya V. Korolkov: 0000-0003-4419-1040

Declaration of Competing Interest

The authors declare no competing interests.

Acknowledgments

This work was partly supported by the Russian Science Foundation under grant No. 16-19-00002 (PL with PLE measurements, quantum chemical simulations), and partly supported by the ISP SB RAS state research program, project No. 0306-2019-0005 (Raman, TSL and XRL spectroscopy). The simulations were performed using computing clusters of the Rzhanov Institute of Semiconductor Physics SB RAS and Novosibirsk State University.

References

[1] C. Århammar, C.M. Araújo, R. Ahuja, Energetics of Al doping and intrinsic defects in monoclinic and cubic zirconia: first-principles calculations, Phys. Rev. B 80 (2009) 115208, doi:10.1103/PhysRevB.80.115208. http://link.aps.org/doi/10.1103/PhysRevB.80.115208.
[2] J. Aarik, H. Mändar, M. Kirm, Spectroscopic characterization of ZrO_2 thin films grown by atomic layer deposition, Proc. Estonian Acad. Sci. Phys. Math. 52 (3) (2003) 289–298.

[3] Y. Arachi, H. Sakai, O. Yamamoto, Y. Takeda, N. Imanishai, Electrical conductivity of the ZrO_2–Ln_2O_3 (Ln=lanthanides) system, Solid State Ion. 121 (1–4) (1999) 133–139, doi:10.1016/s0167-2738(98)00540-2.

[4] M.A. Borik, S.I. Bredikhin, V.T. Bublik, A.V. Kulebyakin, I.E. Kuritsyna, E.E. Lomonova, F.O. Milovich, V.A. Myzina, V.V. Osiko, P.A. Ryabochkina, S.V. Seryakov, N.Y. Tabachkova, Phase composition, structure and properties of $(ZrO_2)_{1-x-y}(Sc_2O_3)_x(Y_2O_3)_y$ solid solution crystals ($x = 0.08$–0.11; $y = 0.01$–0.02) grown by directional crystallization of the melt, J. Cryst. Growth 457 (2017) 122–127, doi:10.1016/j.jcrysgro.2016.06.039.

[5] M.A. Borik, S.I. Bredikhin, V.T. Bublik, A.V. Kulebyakin, I.E. Kuritsyna, E.E. Lomonova, F.O. Milovich, V.A. Myzina, V.V. Osiko, P.A. Ryabochkina, N.Y. Tabachkova, T.V. Volkova, The impact of structural changes in ZrO_2−Y_2O_3 solid solution crystals grown by directional crystallization of the melt on their transport characteristics, Mater. Lett. 205 (2017) 186–189, doi:10.1016/j.matlet.2017.06.059.

[6] M.A. Borik, S.I. Bredikhin, V.T. Bublik, A.V. Kulebyakin, I.E. Kuritsyna, E.E. Lomonova, P.O. Milovich, V.A. Myzina, V.V. Osiko, P.A. Ryabochkina, N.Y. Tabachkova, Structure and conductivity of yttria and scandia-doped zirconia crystals grown by skull melting, J. Am. Ceram. Soc. 100 (2017) 5536–5547, doi:10.1111/jace.15074.

[7] M.A. Borik, S.I. Bredikhin, A.V. Kulebyakin, I.E. Kuritsyna, E.E. Lomonova, F.O. Milovich, V.A. Myzina, V.V. Osiko, V.A. Panov, P.A. Ryabochkina, S.V. Seryakov, N.Y. Tabachkova, Melt growth, structure and properties of $(ZrO_2)_{1-x}(Sc_2O_3)_x$ solid solution crystals ($x = 0.035$–0.11), J. Cryst. Growth 443 (2016) 54–61, doi:10.1016/j.jcrysgro.2016.03.004.

[8] A.N. Chabushkin, A.A. Lyapin, P.A. Ryabochkina, O.L. Antipov, S.A. Artemov, E.E. Lomonova, CW and Q-switched 2 μm solid-state laser on ZrO_2–Y_2O_3–HO_2O_3 crystals pumped by a Tm fiber laser, Laser Phys. 28 (3) (2018) 035803, doi:10.1088/1555-6611/aa962f.

[9] A.S. Foster, V.B. Sulimov, F.L. Gejo, A.L. Shluger, R.M. Nieminen, Structure and electrical levels of point defects in monoclinic zirconia, Phys. Rev. B 64 (2001) 224108, doi:10.1103/PhysRevB.64.224108. https://journals.aps.org/prb/abstract/10.1103/PhysRevB.64.224108.

[10] C. Furetta, Handbook of Thermoluminescence, World Scientific, 2003. https://www.ebook.de/de/product/3822187/furetta_claudio_handbook_of_thermoluminescence.html.

[11] P. Giannozzi, O. Andreussi, T. Brumme, O. Bunau, M.B. Nardelli, M. Calandra, R. Car, C. Cavazzoni, D. Ceresoli, M. Cococcioni, N. Colonna, I. Carnimeo, A.D. Corso, S. de Gironcoli, P. Delugas, R.A. DiStasio, A. Ferretti, A. Floris, G. Fratesi, G. Fugallo, R. Gebauer, U. Gerstmann, F. Giustino, T. Gorni, J. Jia, M. Kawamura, H.-Y. Ko, A. Kokalj, E. Küçükbenli, M. Lazzeri, M. Marsili, N. Marzari, F. Mauri, N.L. Nguyen, H.-V. Nguyen, A.O.-d.l. Roza, L. Paulatto, S. Poncé, D. Rocca, R. Sabatini, B. Santra, M. Schlipf, A.P. Seitsonen, A. Smogunov, I. Timrov, T. Thonhauser, P. Umari, N. Vast, X. Wu, S. Baroni, Advanced capabilities for materials modelling with Quantum ESPRESSO, J. Phys.: Condens. Matter 29 (46) (2017) 465901, doi:10.1088/1361-648x/aa8f79.

[12] V.A. Gritsenko, D.R. Islamov, T.V. Perevalov, V.S. Aliev, A.P. Yelisseyev, E.E. Lomanova, V.A. Pustovarov, A. Chin, The oxygen vacancy in Hafnia as a blue luminescence center and a trap of charge carriers, J. Phys. Chem. C 120 (2016) 19980–19986, doi:10.1021/acs.jpcc.6b05457. http://pubs.acs.org/doi/abs/10.1021/acs.jpcc.6b05457.

[13] V.A. Gritsenko, T.V. Perevalov, D.R. Islamov, Electronic properties of hafnium oxide: a contribution from defects and traps, Phys. Rep. 613 (2016) 1–20, doi:10.1016/j.physrep.2015.11.002.

[14] D.R. Hamann, Optimized norm-conserving vanderbilt pseudopotentials, Phys. Rev. B 88 (2013) 085117, doi:10.1103/physrevb.88.085117.

[15] D.R. Hamann, Erratum: optimized norm-conserving vanderbilt pseudopotentials [Phys. Rev. B 88, 085117 (2013)], Phys. Rev. B 95 (2017) 239906, doi:10.1103/physrevb.95.239906.

[16] Hintersehr, J. (1997). Process for Producing Dental Prostheses. http://www.google.com/patents/US5702650.

[17] J.-H. Hur, S. Park, U.I. Chung, First principles study of oxygen vacancy states in monoclinic ZrO_2: interpretation of conduction characteristics, J. Appl. Phys. 112 (11) (2012) 113719, doi:10.1063/1.4768894.

[18] D.R. Islamov, V.A. Gritsenko, V.N. Kruchinin, E.V. Ivanova, M.V. Zamoryanskaya, M.S. Lebedev, The evolution of the conductivity and cathodoluminescence of the films of hafnium oxide in the case of a change in the concentration of oxygen vacancies, Phys. Solid State 60 (10) (2018) 2050–2057, doi:10.1134/s1063783418100098.

[19] D.R. Islamov, V.A. Gritsenko, T.V. Perevalov, V.S. Aliev, V.A. Nadolinny, A. Chin, Oxygen vacancies in zirconium oxide as the blue luminescence centresand traps responsible for charge transport: Part II — films, Materialia (2020) (Accepted in Materialia as MTLA_100980).

[20] D.R. Islamov, V.A. Gritsenko, T.V. Perevalov, V.A. Pustovarov, O.M. Orlov, A.G. Chernikova, A.M. Markeev, S. Slesazeck, U. Schroeder, T. Mikolajick, G.Y. Krasnikov, Identification of the nature of traps involved in the field cycling of $Hf_{0.5}Zr_{0.5}O_2$-based ferroelectric thin films, Acta Mater. 166 (2019) 47–55, doi:10.1016/j.actamat.2018.12.008. https://www.sciencedirect.com/science/article/pii/S1359645418309509.

[21] T. Ito, H. Kato, Y. Ohki, Mechanisms of several photoluminescence bands in hafnium and zirconium silicates induced by ultraviolet photons, J. Appl. Phys. 99 (2006) 094106, doi:10.1063/1.2199977.

[22] T. Ito, M. Maeda, K. Nakamura, H. Kato, Y. Ohki, Similarities in photoluminescence in hafnia and zirconia induced by ultraviolet photons, J. Appl. Phys. 97 (5) (2005) 054104, doi:10.1063/1.1856220.

[23] E.V. Ivanova, M.V. Zamoryanskaya, V.A. Pustovarov, V.S. Aliev, V.A. Gritsenko, A.P. Yelisseyev, Cathodo- and photoluminescence rise in amorphous hafnium oxide at annealing in oxygen, JETP 120 (4) (2015) 710–715, doi:10.1134/S1063776115020132.

[24] G. Kitis, J.M. Gomez-Ros, J.W.N. Tuyn, Thermoluminescence glow-curve deconvolution functions for first, second and general orders of kinetics, J. Phys. D: Appl. Phys. 31 (19) (1998) 2636–2641, doi:10.1088/0022-3727/31/19/037.

[25] A. Kokalj, XCrySDen—a new program for displaying crystalline structures and electron densities, J. Mol. Graph. Model. 17 (3-4) (1999) 176–179, doi:10.1016/s1093-3263(99)00028-5.

[26] Y.S. Kuz'minov, E.E. Lomonova, V.V. Osiko, Cubic Zirconia and Skull Melting, Cambridge International Science Publishing Ltd, 2008. https://www.ebook.de/de/product/5273548/yurii_sergeevich_kuz_minov_elena_evgen_evna_lomonova_vyacheslav_vasil_evich_osiko_cubic_zirconia_and_skull_melting.html.

[27] D. Mehta, R. Shetty, Bonding to zirconia: elucidating the confusion, Int. Dent. S. Afr. 12 (2) (2010) 46.

[28] V.V. Osiko, E.E. Lomonova, Multifunctional materials based on nanostructured partially stabilized zirconia crystals, Herald Russian Acad. Sci. 82 (5) (2012) 373–382, doi:10.1134/s1019331612050036.

[29] T.V. Perevalov, V.S. Aliev, V.A. Gritsenko, A.A. Saraev, V.V. Kaichev, E.V. Ivanova, M.V. Zamoryanskaya, The origin of 2.7 eV luminescence and 5.2 eV excitation band in hafnium oxide, Appl. Phys. Lett. 104 (2014) 071904, doi:10.1063/1.4865259.

[30] T.V. Perevalov, D.V. Gulyaev, V.S. Aliev, K.S. Zhuravlev, V.A. Gritsenko, A.P. Yelisseyev, The origin of 2.7 eV blue luminescence band in zirconium oxide, J. Appl. Phys. 116 (2014) 244109, doi:10.1063/1.4905105.

[31] T.V. Perevalov, D.R. Islamov, Atomic and electronic structure of oxygen polyvacancies in ZrO_2, Microelectron. Eng. 178 (2017) 275–278, doi:10.1016/j.mee.2017.05.036. http://www.sciencedirect.com/science/article/pii/S0167931717302332.

[32] T.V. Perevalov, D.R. Islamov, Oxygen polyvacancies as conductive filament in zirconia: first principle simulation, ECS Trans. 80 (2017) 357–362, doi:10.1149/08001.0357ecst. http://ecst.ecsdl.org/content/80/1/357.

[33] G. Pezzotti, A.A. Porporati, Raman spectroscopic analysis of phase-transformation and stress patterns in zirconia hip joints, J. Biomed. Opt. 9 (2) (2004) 372.

[34] A.A. Rastorguev, V.I. Belyi, T.P. Smirnova, L.V. Yakovkina, M.V. Zamoryanskaya, V.A. Gritsenko, H. Wong, Luminescence of intrinsic and extrinsic defects in hafnium oxide films, Phys. Rev. B 76 (2007) 235315, doi:10.1103/PhysRevB.76.235315.

[35] P.A. Ryabochkina, M.A. Borik, A.V. Kulebyakin, E.E. Lomonova, A.V. Malov, N.V. Somov, S.N. Ushakov, A.N. Chabushkin, E.V. Chuprunov, Structure and spectral-luminescence properties of yttrium-stabilized zirconia crystals activated with Tm^{3+} ions, Optics Spectrosc. 112 (4) (2012) 594–600, doi:10.1134/s0030400x12030174.

[36] F. Singh, M. Rawat, S.K. Gautam, S. Ojha, Micro-raman investigations on zirconium oxide film during swift heavy ion irradiation to study crystalline-to-crystalline phase transformation kinetics by cascade overlap model, J. Appl. Phys. 126 (2019).

[37] K. Smits, L. Grigorjeva, D. Millers, A. Sarakovskis, J. Grabis, W. Lojkowski, Intrinsic defect related luminescence in ZrO_2, J. Lumin. 131 (10) (2011) 2058–2062, doi:10.1016/j.jlumin.2011.05.018. http://www.sciencedirect.com/science/article/pii/S0022231311002808.